**RESEARCH**

# Investigation of Solvent Effect and H-Bonding on Spectroscopic Properties of 1-(3-Amino-6-(2,5-dichlorothiophen-3-yl)-4-phenylfuro[2,3-b]Pyridin-2-yl) Ethenone: Experimental and Computational Study

Rasha K. Abuflaha[1] · Fakhri O. Yousef[2] · Raed Ghanem[1] · Khaldoun Al-Sou'od[1] · Ihsan A. Shahdi[3] · Omar K. Almashaqbeh[1] · Mahmoud Al-Refai[1]

## Abstract

The furo[2,3-b]pyridine moiety is an important scaffold for many biologically active compounds, therefore, the spectral data of the derivative 1-(3-Amino-6-(2,5-dichlorothiophen-3-yl)-4-phenylfuro[2,3-b]pyridin-2-yl) ethenone (FP1) were investigated. Analysis of absorption-pH profile and Förster cycle of FP1 revealed that its excited state is more acidic than its ground state ($pK_a^* < pK_a$). The main fluorescence emission band of FP1 at 480 nm (in hexane) is shifted to longer wavelengths with increasing polarities of solvents. Linear Lippert's plot and linear correlation between bands maxima and Camlet-Taft parameter, α, of the protic solvents indicated efficient intramolecular charge transfer and noticeable H-bonding. Moreover, the disappearance of the absorption band of FP1 at 385 nm in water, along with the noticeable red shift and quenching of the emission band, and the lower lifetime, relative to nonaqueous solvents, indicate the interruption of the furo[2,3-b]pyridine aromatic moiety. In addition, results from the Time Dependent Density Functional Theory (TDDFT) and Molecular Mechanic (MM) calculations were in agreement with experimentally determined spectra of FP1.

**Keywords** Furo[2,3-b]pyridine · Fluorescence Spectral Analysis · Förster Cycle Analysis · Lippert's Plot · Excited State H-bonding · TDDFT Calculations

## Introduction

The heterocyclic furo[2,3-b]pyridine moiety is increasingly attracting interest as an important scaffold for many biologically and pharmacologically active compounds. Many of the reported furo[2,3-b]pyridine chemical entities showed unique biological activities as kinase inhibitors and exhibited promising pharmacological activity as anticancer and anti-microbial agents [1–6]. Recently, Al-Refai et al. reported the synthesis of furo[2,3-b]pyridine derivatives of new 4-aryl-2-(2-oxopropoxy)-6-(2,5-dichlorothiophene) nicotinonitrile as potent antioxidant agents [7]. The basic compound of these derivatives is 1-(3-Amino-6-(2,5-dichlorothiophen-3-yl)-4-phenylfuro[2,3-b]pyridin-2-yl) ethenone (FP1) (Fig. 1), and other derivatives were obtained by changing the phenyl group at position 4 with different aryl derivatives. Therefore, understanding the photophysical properties of FP1 may present a step ahead in understanding the excited state properties of these furo[2,3-b]pyridine compounds.

Although the 4-substituted furo[2,3-b]pyridine dyes (polymethine dyes) were synthesized by Abramenko et al. in the seventies of the previous century [8], the exploration of the photophysical properties of the furo[2,3-b]pyridine derivatives is still at its minimum. Furo[2,3-b]pyridine ring moiety is a combination of π-electron rich furan ring and a π-electron deficient pyridine ring [9], therefore, its derivatives are expected to show photo-illumination activities.

✉ Raed Ghanem
  raedag@aabu.edu.jo

1  Department of Chemistry, Al al-Bayt University, Mafraq, Jordan

2  Department of Chemistry, Al-Hussein Bin Talal University, Ma'an, Jordan

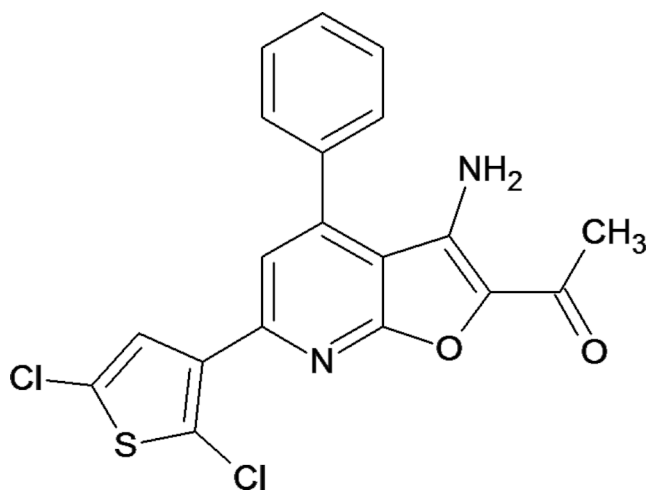3  Department of Chemistry, Pure and Applied Chemistry Group, University of Sharjah, P.O. Box 27272, Sharjah, UAE

**Fig. 1** Structure of FP1: 1-(3-Amino-6-(2,5-dichlorothiophen-3-yl)-4-phenylfuro[2,3-b]pyridin-2-yl) ethenone

However, only few fluorescence and phosphorescence articles based on furo[2,3-b]pyridine derivatives are reported [10–12].

In this work, the photophysical properties of FP1 are investigated, in order to understand the excited state properties of these furo[2,3-b]pyridine compounds. This includes experimental and computational investigations of solvatochromism, H-bonding effects on fluorescence emission spectra of FP1 and evaluation of excited state dissociation constant $pK_a^*$.

## Experimental

### Materials and Experimental Procedures

Compound FP1 was synthesized, and characterized by [1] H-NMR, in accordance with the reported method [7] and used without any further purification and all other chemicals were Sigma-Aldrich analytical grade reagents. Aqueous solutions were prepared using spectroscopic grade water purchased from Merck and used as received. Solutions for spectroscopic measurements contained a fixed concentration of FP1 ($1.33 \times 10^{-5}$ mol dm$^{-3}$). The ground and excited state acid dissociation constants of FP1 were determined through analysis of absorption and fluorescence emission pH profiles. Solutions of pH profiles were aqueous 0.1 mol L$^{-1}$ phosphate buffer solutions within the pH range of 1–13. All fluorescence measurements were made according to a previously described method [13]. [1] H-NMR spectrum of FP1 was obtained in a mixture of H$_2$O:DMSO-d$_6$ (5:95 by volume) at 25 °C for H-bonding investigations.

An exponential growth or decay process was expressed in mathematical terms R(t)

$$R(t) = \sum B_i \exp\left(-\frac{t}{\tau_i}\right) \tag{1}$$

Where R(t) is the sample decay model. R(t) is a theoretical expression for the response of the sample to an infinitely short excitation. $B_i$ are amplitudes and $\tau_i$ are the lifetimes. The fluorescence lifetime was obtained through the analysis of the sample decay model. Fluorescence decay was acquired to $10^4$ counts in the peak. The decays were repeated at least three times and fitted according to Eq. 1. Decay curves were analyzed by using single or double exponentials. The goodness of the individual fits was judged by the magnitude of $\chi^2$ and the shape of the autocorrelation function of the weighted residuals.

### Instruments

The UV–visible absorption measurements were made using a Specord, S-600 diode array spectrophotometer. Emission spectra were collected using the FL 900 S spectrofluorometer from Edinburg Analytical Instruments equipped with time correlated single photon counting on FL-900CD, with the excitation provided by a nanosecond nF900 flash lamp filled with H$_2$ at 0.4 bars, and operating at 40 kHz, with 6 KV applied across a 1 mm electrode gap.

[1] H-NMR spectrum of FP1 was obtained on a Bruker [ultra-shield 300 MHz] spectrometer and chemical shifts (δ) expressed in ppm were measured with reference to TMS.

### Molecular Mechanics Calculations

Molecular mechanics (MM) studies were performed in vacuum and in water to predict the formation of intramolecular H-bonding within FP1 molecules and intermolecular H-bonding between two FP1 molecules (dimer) utilizing Hyperchem® software (Release 8.06, Hypercube, Inc. USA). The force fields Amber94, enhanced MM, BIO+ (CHARMM) and OPLS method were used in the calculations of hydrogen-bonded interactions, while partial atomic charges were obtained by performing AM1 semi-empirical calculations. Aqueous solvation effects were also achieved by using the Polak-Rebiere algorithm (PR), which rapidly packs solvents molecules around the solute. Initially, energy minimizations were obtained using the Polak-Rebiere algorithm (0.1 kcal/mol.A) gradient. FP1 was built up from natural bond angles, as defined in this software, and structures were then minimized with the MM, Amber, BIO+ (CHARMM) and OPLS force field, the resulting structure was further optimized at the HF-ab initio level with the 3-21G basis set (310 basis functions were used with 507 primitive Gaussians). In addition, Density Functional Theory and time dependent Density functional theory (TDDFT)

methods were further used to provide an insight into the ground and excited states of FP1 in vacuum and in water. The structure of FP1 was optimized at the level of theory B3LYP using 6–31(g) basis set. The single point energies along with UV-vis absorptions were determined at the same level of theory with higher basis set of 6-311G (2d,p) [14]. The solvation model used in the single point energy calculations of the gas phase (ground and excited states) was the self-consistent reaction field (SCRF) with integral equation formalism polarizable continuum model (IEPCM). All DFT calculations were conducted using G16 (Linux) through input files prepared by GV6 software [15, 16].

## Results and Discussion

### Spectroscopic and Photophysical Characteristics of Compound FP1

The UV-visible spectra of FP1 in selected solvents of different polarities are shown in Fig. 2. The characteristic absorption bands in the region 250 to 390 nm, are attributed to $\pi \rightarrow \pi^*$ and $n \rightarrow \pi^*$ transitions within the furo-pyridine portion, which are in a good agreement with the reported literature on similar fragments (Fig. 2) [11, 17, 18]. Absorption bands at about 280 and 340 nm can be assigned to the phenyl-furo[2,3-b]pyridine moiety, while the shoulder at about 385 nm is believed to be induced by an intramolecular H-bonding between the amino hydrogens and the carbonyl oxygen in FP1. The position of the absorption bands does not show any clear relation to solvent polarity, except with water, where dramatic changes are observed. The fluorescence emission spectrum of FP1 contains only one characteristic band at 480 nm (in hexane) and shifts progressively to longer wavelengths (red shifts) with increasing solvent polarity (Table 1).
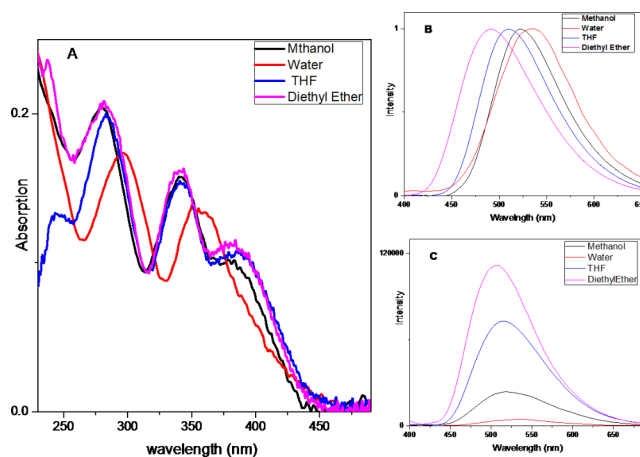


**Fig. 2** A) Absorption bands of $1.33 \times 10^{-5}$ mol/L FP1 in diethyl ether, THF, methanol and water at 25 °C. B) Change of position of normalized emission bands of FP1 with polarity of solvents. C) Change of Fluorescence intensity of FP1 with polarity of solvents. $\lambda_{ex} = 370$ nm

Ground-state acid dissociation constant of FP1 was determined through analysis of the absorbance-pH profile, Fig. 3, with $pK_a$ taken equal to the pH value at the inflection point of the sigmoidal curve of the absorbance at $\lambda = 350$ nm against pH values. Results reveal that $pK_a = 4.7 \pm 0.2$ ($R^2 = 0.95$), which can be assigned to the pyridine nitrogen of the furo-pyridine fragment of FP1 [11]. The excited state acid dissociation constant, $pK_a^*$, is determined through fitting of the experimental emission intensity-pH profile which reveals that $pK_a^* = 3.9 \pm 0.2$ ($R^2 = 0.99$). ), Fig. 3a. Moreover, the increased excited state acidity is also ascertained through Förster cycle analysis utilizing the Eqs. [19, 20]:

$$pK_a^* - pK_a = 0.0021(\bar{\nu}_B - \bar{\nu}_{HB^+}) \tag{2}$$

where the wavenumbers $\bar{\nu}_B$ and $\bar{\nu}_{HB^+}$ corresponding to the 0–0 transitions of the basic and acidic forms of FP1 and usually estimated through the equation [21]:

**Table 1** Solvent parameters and spectral data of FP1 in different solvents at 25°C.

| Solvent | $\varepsilon^a$ | $n^a$ | $\lambda_1$ | $\lambda_2$ | $\lambda_3$ | $\lambda_{em}$ |
|---|---|---|---|---|---|---|
| Water | 78.36 | 1.333 | 293 | 354 | - | 535 |
| Methanol | 32.66 | 1.327 | 279 | 340 | 384 | 520 |
| Ethanol | 24.55 | 1.359 | 280 | 341 | 387 | 510 |
| Butanol | 17.51 | 1.397 | 281 | 343 | 386 | 505 |
| Acetonitrile | 35.94 | 1.341 | 279 | 338 | 383 | 515 |
| Dichloromethane | 8.93 | 1.421 | 280 | 345 | 383 | 500 |
| THF | 7.58 | 1.405 | 282 | 340 | 387 | 510 |
| Ethyl acetate | 6.02 | 1.370 | 280 | 338 | 383 | 510 |
| Chloroform | 4.89 | 1.442 | 282 | 345 | 386 | 495 |
| Diethyl ether | 4.20 | 1.350 | 282 | 336 | 385 | 490 |
| Cyclohexane | 2.02 | 1.424 | 282 | 342 | 386 | 485 |
| n-Hexane | 1.88 | 1.372 | 282 | 342 | 386 | 480 |

[a] Properties of Solvents [27].

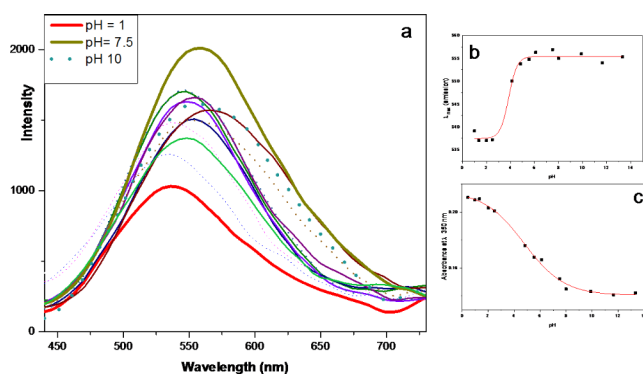**Fig. 3** (a) Emission pH profile of FP1. λexcitation = 370 nm. pH 1, 7.5 and 10 are highlighted (b) Sigmoidal fitting of Emission-pH profile of FP1. (c) Sigmoidal fitting of absorption-pH profile of FP1. Absorbance measured at λ = 350 nm

$$\bar{\nu}_{00} = \frac{\bar{\nu}_{abs}^{max} + \bar{\nu}_{em}^{max}}{2} \tag{3}$$

According to Förster cycle analysis, the calculated $pK_a^*$ value is found to be $3.9 \pm 0.2$, which confirms that FP1 is more acidic in the excited state as reflected by the red shift of the emission band of the basic form ($\lambda_{em} = 560$ nm at pH > 5) relative to the acidic form of FP1 ($\lambda_{em} = 536$ nm at pH < 2.5). This shows that, in the excited state, nitrogen of furo[2,3-b]pyridine moiety is less basic indicating that nitrogen lone pair is presumably involved in the intramolecular charge transfer.

## Solvatochromic Effects

Inspection of the absorption spectra of FP1 in nonpolar, aprotic polar, and protic polar solvents (except water), shows that the position of the absorption bands does not show any clear relation to solvent polarity. In water, the absorption bands of FP1 at about 280 nm ($\lambda_1$) and 340 nm ($\lambda_2$) are noticeably red shifted to 293 and 354 nm respectively. The absorption band (shoulder) at about 385 nm disappears completely as a result, presumably, of strong H-bonding (Fig. 2). Emission spectra of FP1 in different

solvents show an obvious red shift of the emission band from 480 to 520 nm with increasing polarity in accordance with the expected solvatochromic effect (Fig. 2; Table 1). In water, the emission band of FP1 is shifted to 535 nm with a diminished intensity of the fluorescence emission.

Investigation of the changes in ground state and excited state dipole moments upon excitation, can provide useful information about their corresponding electronic distribution. Moreover, solvatochromic data can provide information about the involved electronic transitions, namely, $\pi \to \pi^*$ or $n \to \pi^*$. The change of dipole moment of FP1 upon excitation can be estimated through the Lippert-Mataga Eqs. [21–26],

$$\bar{\nu}_a - \bar{\nu}_f = \left[ \frac{2}{hca^3} (\mu_e - \mu_g)^2 \right] \Delta f + constant \tag{4}$$

where $\bar{\nu}_a - \bar{\nu}_f$ is the stokes shifts, $\mu_e - \mu_g$ is the charge transfer dipole moment of FP1, $a$ is the Onsager radius of solute molecule (radius of solvent cavity), $h$ is Blank's constant, $c$ is speed of light in vacuum, and $\Delta f$ is the orientation polarizability of the solvent, defined by

$$\Delta f = \frac{\epsilon - 1}{2\epsilon + 1} - \frac{n^2 - 1}{2n^2 + 1} \tag{5}$$

where ε and $n$ are the dielectric constant and refractive index of solvents respectively [27]. The calculated orientation polarizability and stokes shifts (in $cm^{-1}$) of FP1 in different solvents are shown in Table 2.

Solvatochromic effect can be evaluated by plotting $\bar{\nu}_a - \bar{\nu}_f$ (stokes shifts) vs. $\Delta f$ for various solvents of different polarities (Lippert's plot), which should show linear trend, if H-bonding is not significant. Data in Fig. 4 clearly shows that solvents polarities are linearly related to stokes shifts ($R^2 = 0.83$) with positive slope indicating an increase of dipole moment of FP1 upon excitation, i.e. ($\mu_e - \mu_g$) is positive, and a corresponding efficient intramolecular charge transfer (ICT) (Fig. 4). Consequently, this linear correlation shows that the microenvironment of FP1 has an important

**Table 2** Solvatochromic data of FP1 (in $cm^{-1}$) and the calculated orientation polarizability of different solvents at 25 °C

| Solvent | $\bar{\nu}_1$ | $\bar{\nu}_e$ | $\Delta\bar{\nu}\ (\bar{\nu}_1 - \bar{\nu}_e)$ | $\Delta f$ |
|---|---|---|---|---|
| Ethanol | 35714 | 19417 | 16297 | 0.290 |
| Butanol | 35587 | 19608 | 15979 | 0.264 |
| Acetonitrile | 35842 | 19608 | 16234 | 0.305 |
| Dichloromethane | 35714 | 20000 | 15714 | 0.218 |
| THF | 35461 | 19608 | 15853 | 0.210 |
| Ethyl acetate | 35714 | 19802 | 15912 | 0.201 |
| Chloroform | 35461 | 20202 | 15259 | 0.149 |
| Diethyl ether | 35461 | 20202 | 15259 | 0.163 |
| Cyclohexane | 35461 | 20619 | 14842 | 0.000 |
| Hexane | 35461 | 20619 | 14842 | 0.000 |

impact on its spectral properties. These solvatochromic data indicate that a bathochromic shift is observed with increasing polarity of the solvents, confirming a $\pi \rightarrow \pi^*$ transition [25, 26]. It should be pointed out that water and methanol are not included in the Lippert's plot, because of the strong H-bonding they can form according to their large Camlet-Taft parameter, α, of the protic solvents [28, 29]. Lippert-Mataga model, is based mainly on dipole-dipole interactions and H-bonding can deviate their corresponding plots from linearity.

### H-bonding Effects

In nonpolar solvents and aprotic polar solvents, FP1 may form intramolecular H-bonding between the amino hydrogens and the carbonyl oxygen, therefore, existing in two conformers (FP1-a and FP1-b) under equilibrium, Scheme. 1 in accordance with reported literature [11]. The reported ^{1}H-NMR of FP1 in CDCl₃ shows that the chemical shift
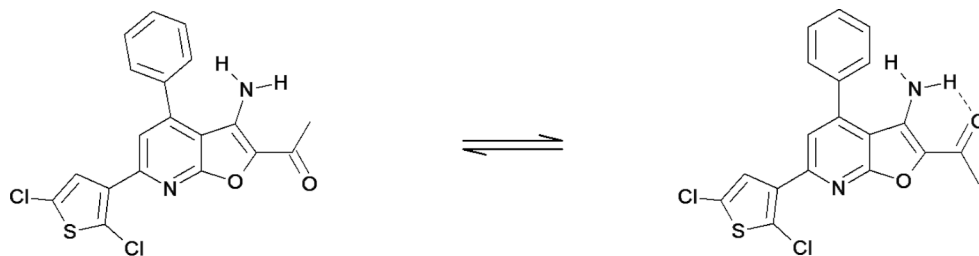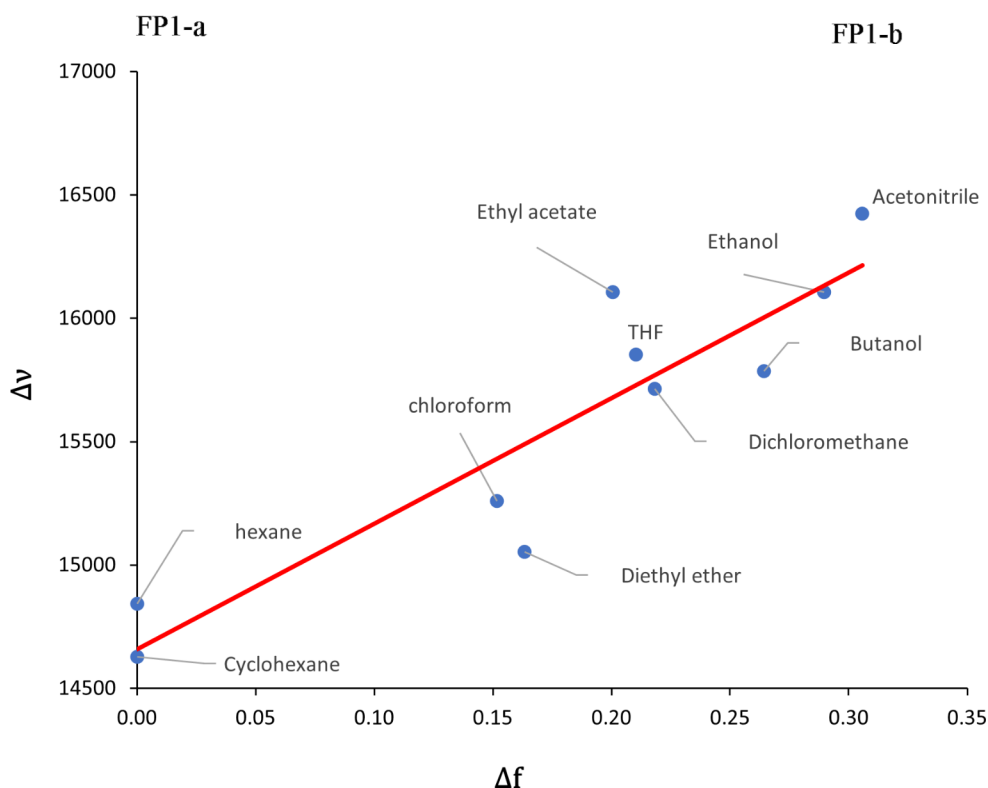
of the amino group protons appears as a splitted singlet at about 5.1 ppm [7]. This downfield chemical shift of the amino group protons and the splitted singlet clearly confirms this intramolecular H-bonding. The existence of intermolecular H-bonding between the amino hydrogens and the carbonyl oxygen on two different FP1 moieties cannot also be excluded, forming a sort of non-bonded dimer. Moreover, protic polar solvents, like alcohols, can form H-bonding to Hydrogen Bond Acceptor (HBA) groups in FP1 like the pyridine nitrogen and the carbonyl oxygen in addition to the existing intramolecular H-bonding. Enhanced intramolecular charge transfer (ICT) with increasing the polarity of the solvents in addition to the intramolecular and intermolecular H-bonding causes the progressively red shift of the fluorescence emission band from 480 nm (in hexane) to 520 nm (in methanol) (Fig. 2) [11, 30–34].

Water can break the intramolecular H-bonding and form strong intermolecular H-bonding with FP1 [11]. This effect of water is confirmed through the ^{1}H-NMR spectrum of

Scheme 1



impact on its spectral properties.

Fig. 4 Lippert's plot of FP1 in different solvents

FP1, obtained in $H_2O$:DMSO-$d_6$ (5:95 by volume), that shows a downfield chemical shift displacement of the singlet of the amino group protons from 5.1 ppm, in CDCl$_3$, to 5.8 ppm. Moreover, the splitted singlet, in CDCl$_3$, changed into a symmetrical singlet, in $H_2O$:DMSO-$d_6$ mixture, (Fig. 5) indicating the formation of a stronger intermolecular H-bonding of FP1 with water and DMSO. As another evident of claim, is the disappearance of the shoulder at about 385 nm in the absorption spectrum of FP1 in water, and the large red shift and large depletion of intensity of the emission band relative to polar aprotic or protic solvents (Fig. 2). In order to confirm these effects of water, further

experiments are performed where the absorption and emission spectra of FP1 are obtained in methanol with gradual addition of water (0–80%) (Fig. 6). Inspection of Fig. 6 clearly shows the gradual red shift of FP1 absorption bands and the gradual quenching of the emission intensity upon the addition of water and complete disappearance of the absorption band at 385 nm in 80% water/methanol solution. FP1 has two HBA groups, namely, the conjugated carbonyl-amine moiety and the pyridine moiety. Therefore, FP1 is expected to form noticeable H-bonding with protic solvents. However, we believe that the structure of conjugated carbonyl-amine moiety with the separated charges, Scheme. 2,
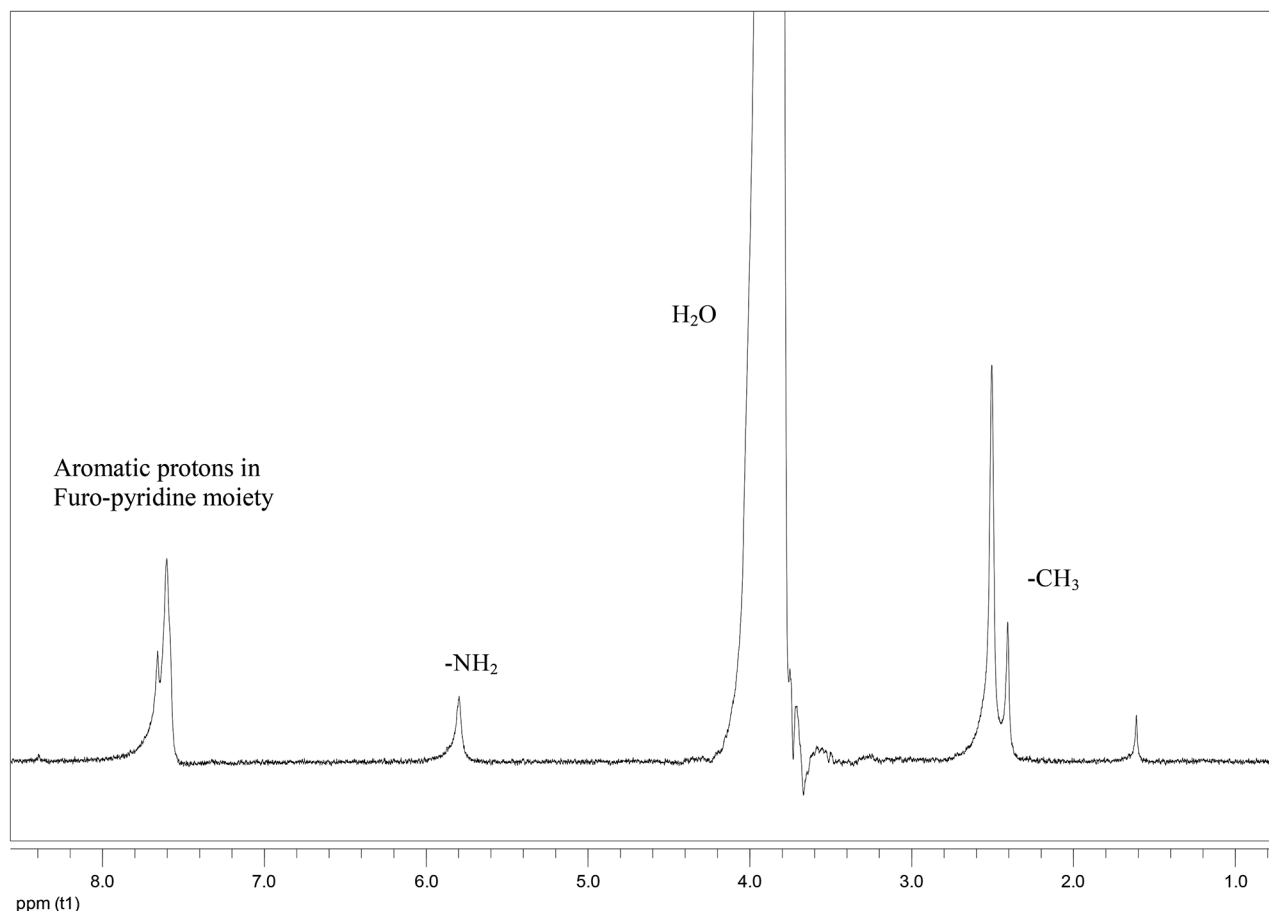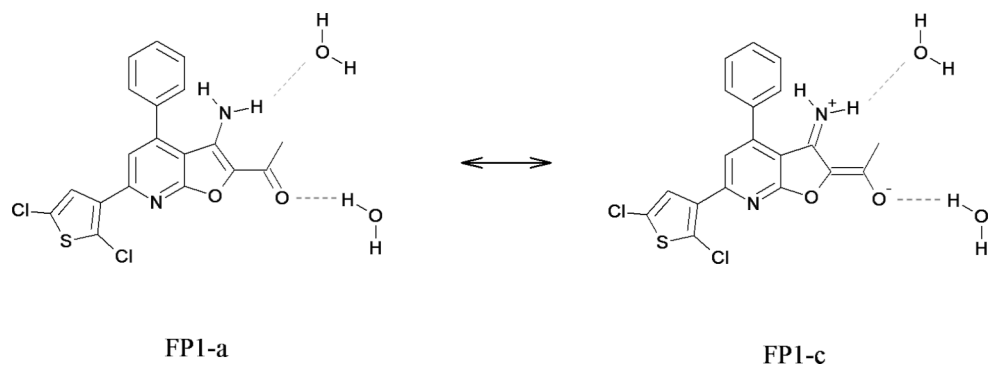
Scheme 2



FP1-a                                    FP1-c



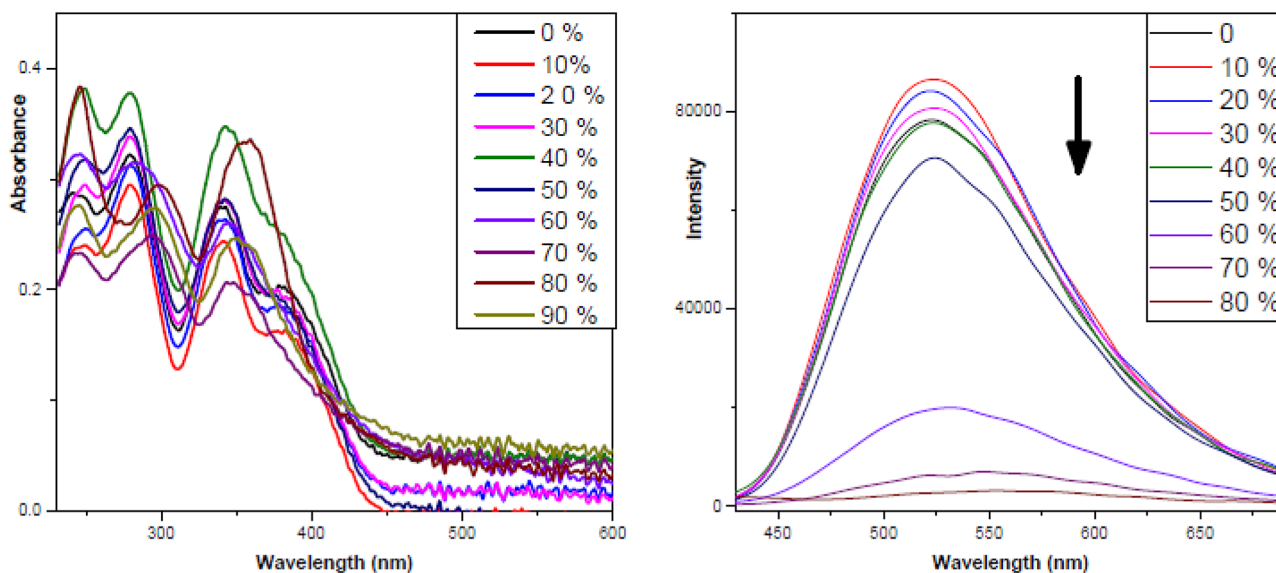**Fig. 5** $^1$H-NMR spectrum of FP1 obtained in DMSO-$d_6$ at 25 °C. $H_2O$

**Fig. 6** Change of absorption and emission spectra of FP1in methanol upon gradual addition of water at 25 °C

can form stronger and more stabilized H-bonding with water, structure FP1-c. Interestingly, a similar structure is proposed for coumarin derivative in the excited state to explain the observed red shifts in polar protic solvents [28]. Structure FP1-c interrupts the conjugated aromatic system of the furo-pyridine portion as the chromophore is mainly located on the furo[2,3-b]pyridine moiety [11]. Such interruption, in addition to other H-bonding effects of water, leads to the disappearance of the absorption band at 385 nm and diminishes the intensity of fluorescence emission of FP1 (Fig. 2).

The assumption of excited state stabilization by H-bonding is confirmed by the linear correlation of the emission energy of FP1 and the reported Camlet-Taft parameter, α, of the protic solvents [28, 33] (Fig. 7). The negative slope of the linear correlation indicates the lowering of the emission energy, as reflected by increasing of the red shift of the emission band of FP1, with increasing the Hydrogen Bond Donor (HBD), or acidity, character, α, of the protic solvents. The behavior of FP1 as a H-bond doner in the excited state is also investigated through plotting the emission energy of FP1 against the reported Camlet-Taft HBA or basicity character, β, for many protic and aprotic polar solvents [29]. However, no adequate correlation is obtained, confirming the assumption that FP1 behaves mainly as a H-bond acceptor.



**Fig. 7** Correlation of the emission maxima of FP1 (in $cm^{-1}$) with the reported Camlet-Taft parameter, α, of the protic solvents [28]
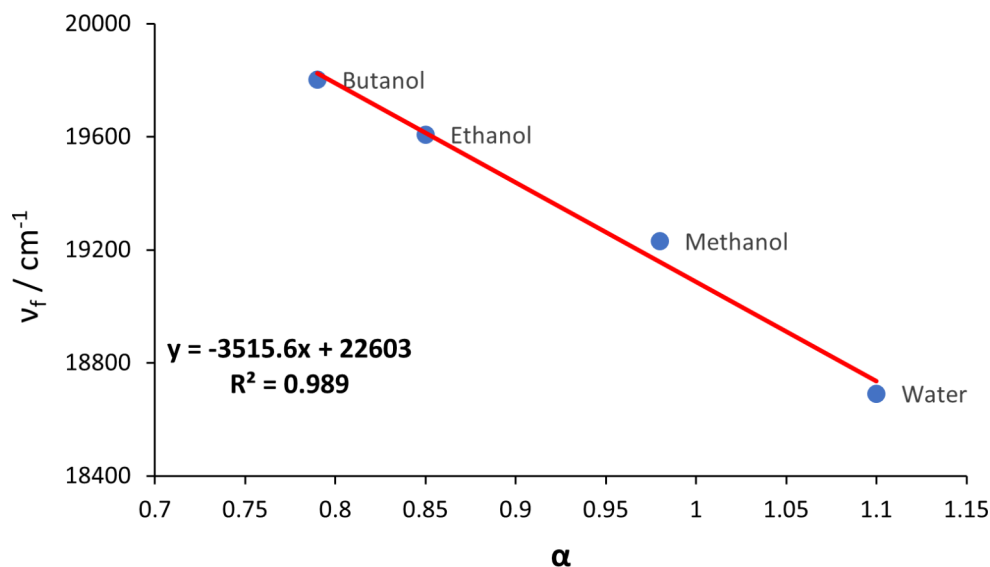
$$y = -3515.6x + 22603$$
$$R^2 = 0.989$$

**Table 3** Average fluorescence lifetimes (ns) and $\chi^2$ values of compound FP1 in selected solvents of different polarities ($\lambda_{ex}$= 370 nm and $\lambda_{em}$ = 520 nm)

| Solvent | $\tau_1$ (ns) | $B_1$ | $\tau_2$ ns | $B_2$ | Average Lifetime <$\tau$> (ns) | $\chi^2$ | Relative concentration of the second component ($C_2$) |
|---|---|---|---|---|---|---|---|
| Diethyl ether | 8.37 | 32,045 | 46.911 | 110 | 9.098 | 1.012 | 0.00342 |
| Chloroform | 7.494 | 39,056 | 45.122 | 130 | 8.233 | 0.922 | 0.00332 |
| Acetonitrile | 7.756 | 23,162 | 43.653 | 96 | 8.574 | 0.899 | 0.00413 |
| Ethyl acetate | 7.762 | 26,481 | 42.598 | 120 | 8.607 | 1.203 | 0.04335 |
| Methanol | 5.261 | 17,838 | 42.051 | 58 | 6.193 | 1.321 | 0.00324 |
| Water | 3.901 | 1545 | - | - | - | 0.992 | - |

B is the Pre-exponential Factor. $<\tau> = \frac{B_1\tau_1^2 + B_2\tau_2^2}{B_1\tau_1 + B_2\tau_2}$ and $C_2 = \frac{B_2}{B_1+B_2}$
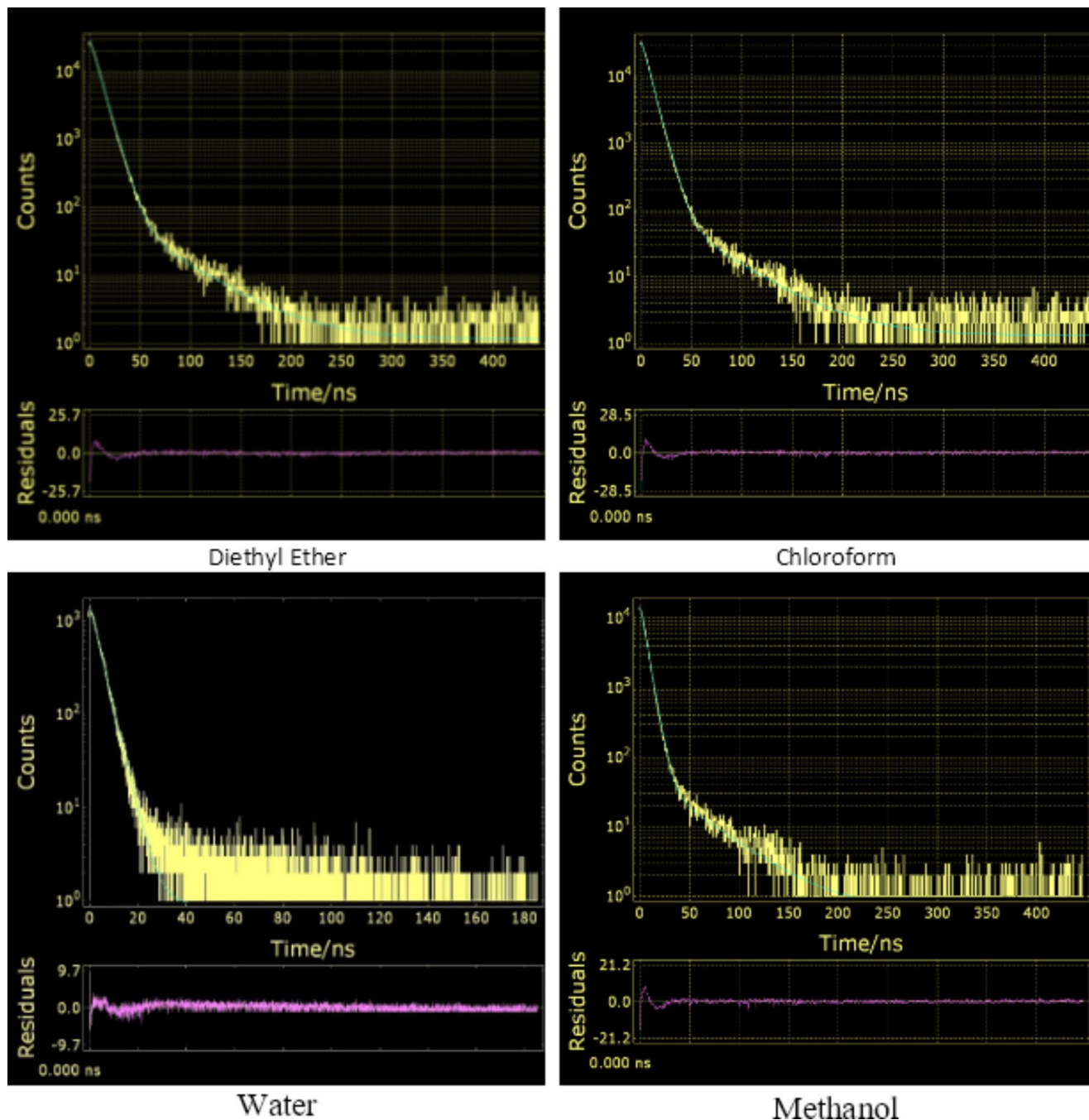


**Fig. 8** Decay of fluorescence emission with time in selected solvents of different polarities

Time-resolved fluorescence measurements carried out for compound FP1 in different solvents, show that, excluding water, the fluorescence decays at 520 nm are satisfactorily fitted to double exponential functions with average lifetimes of about 9.1–8.1 ns with a satisfactorily $\chi^2$ values of 0.9–1.3 (Table 3) (Fig. 8). As the fluorescing chromophore is the furo[2,3-b]pyridine moiety, the constancy of the lifetimes of FP1 in different solvents ascertains that the excited state contains mainly one structure of FP1 with the furo[2,3-b] pyridine moiety unchanged. On the other hand, results show that the fluorescence decays are best fitted to double exponential equation. However, the values of the pre-exponential factor of the second component, $B_2$, reveals that the contribution of the second species is very small (i.e., the relative concentration of the second component ($C_2$) is very small, Table 3). On the other hand, the lifetime of FP1 in water is decreased to 3.9 ns which indicates that the structure of FP1 in the excited state is different from other solvents and that the

furo[2,3-b]pyridine moiety has been changed, confirming our assumption (Scheme 2).

Finally, inspection of spectral results shows that FP1 in methanol exhibited relatively lower intensity of fluorescence emission and larger red shifts than in other solvents (Fig. 2). The lifetime in methanol is found to be 6.1 ns, which is also lower than lifetimes in other solvents but higher than that in water. These results indicate that methanol can make noticeable H-bonding with FP1, however, cannot interrupt its furo[2,3-b]pyridine moiety.

## Molecular Modeling Results

Molecular mechanics calculations, in vacuum, revealed that FP1 can make stable intramolecular H-bonding between the amino hydrogens and the carbonyl oxygen or intermolecular H-bonding between the amino hydrogens and the carbonyl oxygen on different molecules forming a type of non-bonded dimer (Fig. 9). However, minimized structures
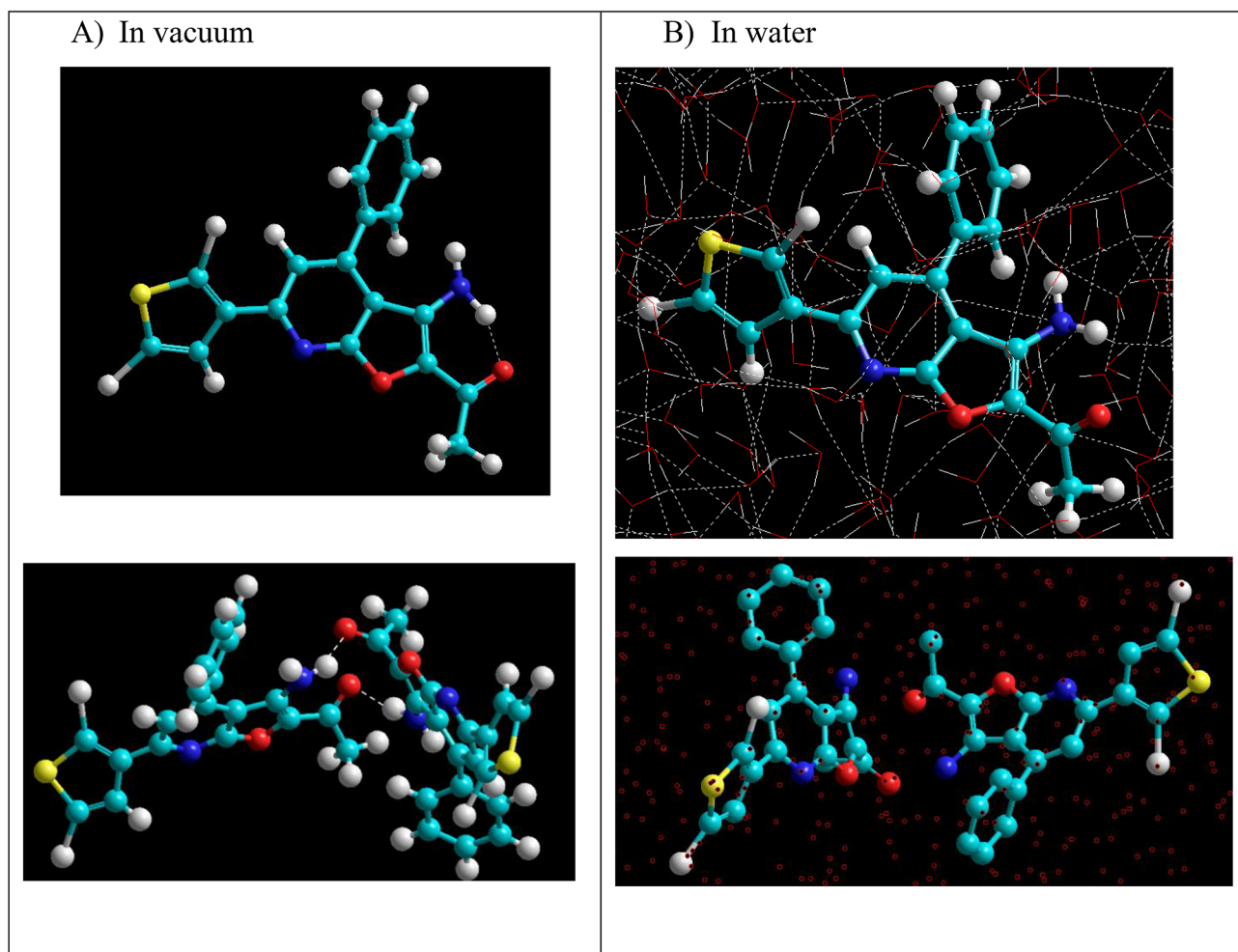


**Fig. 9** Stable structures of FP1 in (A) vacuum and in (B) water as minimized by MM calculations showing intra- and intermolecular H-bonding. *Hydrogen removed for clarity*

of FP1 in water do not show any stable intra- or intermolecular H-bonding, in accordance with spectroscopic data (Fig. 9).

### Results of the DFT and TDDFT Calculations

The total dipole of excited FP1 in vacuum was 5.0125 Debye while in the water was 7.7189, that can be attributed to the H-bonding and/or ICT between FP1 and water (Fig. 10). In addition, the red shift of absorption band at 348 nm in vacuum to 351 nm in water in agreement of experimental shifts observed of bands at 340 to 354 nm (Table 3). Such behavior can be attributed to hydrogen bonding. The solvation

**Table 3** TDDFT Calculated spectral data of FP1 in water and vacuum

| Spectral Property | Wavelength ($\lambda$, nm) | Extinction coefficient $\varepsilon \times 10^4\,M^{-1}.cm^{-1}$ | Oscillator strength | Assigned Transition | Excited state HOMO-n $\rightarrow$ LUMO+n |
|---|---|---|---|---|---|
| In water | 351 | 1.3995 | 0.2631 | $\pi \rightarrow \pi^*$ | 103(HOMO) $\rightarrow$ 104 |
| | 403.8 | 1.3636 | 0.2631 | $\pi \rightarrow \pi^*$ | 102 $\rightarrow$ 104 |
| In vacuum | 348.5 | 8.939 | 0.1506 | $\pi \rightarrow \pi^*$ | 102 $\rightarrow$ 104 103(HOMO) $\rightarrow$ 105 |
| | 407 | 7585.2 | 0.1917 | $\pi \rightarrow \pi^*$ | 103(HOMO) $\rightarrow$ 104 103(HOMO) $\rightarrow$ 105 |



**Fig. 10** (a) Gas phase ESP map of FP1 with Mullikan charge distribution, (b) solvent cavity (water) phase ESP map with Mullikan charge distribution
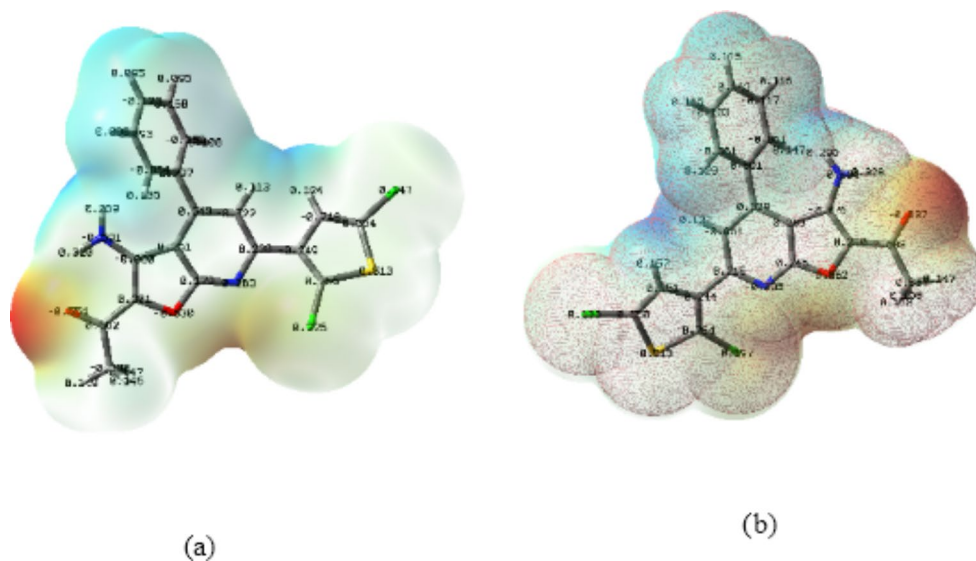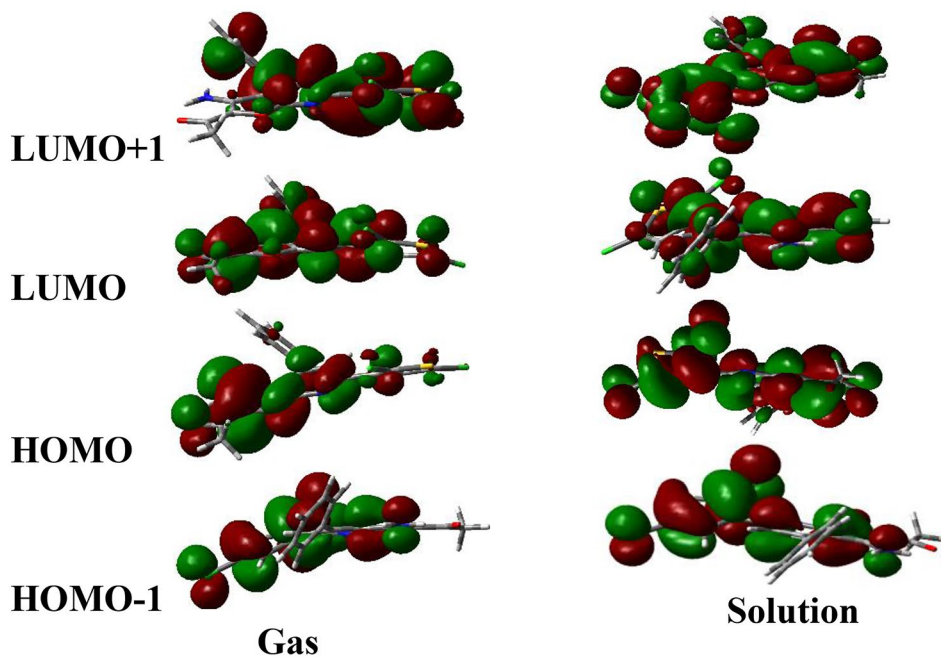
(a)                                                (b)



**Fig. 11** Molecular orbital diagram of the observed singlet transitions in vacuum and in water for FP1

LUMO+1

LUMO

HOMO

HOMO-1

Gas                                                Solution

energy of the excited FP1 in solution is also determined to be − 10.35 kcal/mol. The main characters of the singlet states that were involved in the transition in both vacuum and water were expressed in Fig. 11. The electrostatic potentials (ESP) for both excited states along with Mullikan charge distributions were reported. (Fig. 10). The molecular energy diagrams of both states are also reported. (Fig. 11).

## Conclusion

Analysis of the computational and experimental spectral data of compound FP1 showed that its excited state is more polar than its ground state because of intramolecular charge transfer (ICT) and H-bonding, while Förster cycle analysis showed that the excited state is more acidic than the ground state. Linear Lippert's plot proved a positive solvatochromic effect, while linear correlation between emission maxima and Camlet-Taft parameter, α, of the protic solvents proved the H-bonding contribution. The high fluorescence emission intensity and the constant lifetime of FP1 in different nonaqueous solvents, indicate that the furo[2,3-b]pyridine moiety primarily stay intact in the excited state. In water, the strong H-bonding can interrupt the aromatic system of the furo[2,3-b]pyridine moiety leading to a diminished fluorescence emission intensity and lower lifetime of FP1.

**Author'Contributions** Author Contributions: Raed Ghanem and Fakhri Yousef designed the experiments and controlled the whole project and wrote the manuscript. Rasha K. Abufaha, Omar K. Almashaqbeh and Mahmoud AlRefai prepared the molecules and did the experimental part. Khaldoun Al-Sou'od, Ihsan A. Shahdi did the theoretical calculations. All authors reviewed the manuscript.

**Data Availability** "Not applicable".

## Declarations

**Conflict of interest** The authors declare that there are no conflicts of interest.

**Ethical Approval** This article does not contain any studies with human participants or animals performed by any of the authors Ethics declarations.

## References

1. -Abdel-Rahman AAH, Shaban AKF, Nassar IF, EL-Kady DS, Ismail NSM, Mahmoud SF, Awad HM, El-Sayed WA (2021) Discovery of New Pyrazolopyridine, Furopyridine, and pyridine derivatives as CDK2 inhibitors: design, synthesis, Docking Studies, and anti-proliferative activity. Molecules 26:3923. https://doi.org/10.3390/molecules26133923

2. -Němec V, Hylsová M, Maier L, Flegel J, Sievers S, Ziegler S, Schroeder M, Berger BT, Chaikuad A, Valčá¼ková B, Uldrijan S, Drápela S, Souček K, Waldmann H, Knapp S, Paruch K (2019) Furo[3,2-b]pyridine: a Privileged Scaffold for highly selective kinase inhibitors and effective modulators of the hedgehog pathway. Angew Chem Int Ed 58(4):1062–1066. https://doi.org/10.1002/anie.201810312

3. -Kumar RN, Poornachandra Y, Nagender P, Mallareddy G, Kumar NR, Ranjithreddy P, Kumar CG, Narsaiah B (2016) Synthesis of novel trifluoromethyl substituted furo[2,3-b]pyridine and pyrido[3′,2′:4,5]furo[3,2-d]pyrimidine derivatives as potential anticancer agents. Eur J Med Chem 108:68–78. https://doi.org/10.1016/j.ejmech.2015.11.007

4. -Ibrahim MM, AlRefai M, Azmi MN, Osman H, Abu Bakar MH, Geyer A (2019) Synthesis, characterization and cytotoxicity of new nicotinonitriles and their furo[2,3-b]pyridine derivatives. J Iran CHEM SOC 16:715–722. https://doi.org/10.1007/s13738-018-1549-y

5. -Němec V, Maier L, Berger BT, Chaikuad A, Drápela S, Souček K, Knapp S, Paruch K (2021) Highly selective inhibitors of protein kinases CLK and HIPK with the furo[3,2-b]pyridine core. Eur J Med Chem 215:113299. https://doi.org/10.1016/j.ejmech.2021.113299

6. -Fumagalli F, de Melo SMG, Ribeiro CM, Cristina Solcia M, Rogério Pavan F, da Silva Emery F (2019) Exploiting the furo[2,3-b]pyridine core against multidrug-resistant Mycobacterium tuberculosis. Bioorg Med Chem Lett 29(8):974–977. https://doi.org/10.1016/j.bmcl.2019.02.019

7. -Al-Refai M, Ibrahim M, Al-Fawwaz A, Geyer A (2018) Synthesis and characterization of new 4-aryl-2-(2-oxopropoxy)-6-(2,5-dichlorothiophene)nicotinonitrile and their furo[2,3-b]pyridine derivatives: Assessment of antioxidant and biological activity. Eur J Chem 9(4):375–381. https://doi.org/10.5155/eurjchem.9.4.375-381.1792

8. -Abramenko PI, Zhiryakov VG, Ponomareva TK (1976) Polymethine dyes – 4-substituted furo [2,3-b]- and selenopheno[2,3-b] pyridine derivatives. Chem Heterocycl Compd 12:52–56. https://doi.org/10.1007/BF00473913

9. -Chartoire A, Comoy C, Fort Y (2008) Furo[3,2-b]pyridine: a convenient unit for the synthesis of polyheterocycles. Tetrahedron 64(48):10867–10873. https://doi.org/10.1016/j.tet.2008.09.008

10. -Lee CW, Lee JY (2013) Highly electron deficient pyrido[3',2':4,5]furo- [2,3-b]pyridine as a core structure of a triplet host material for high efficiency green phosphorescent organic light-emitting diodes. Chem Commun 49:6185–6187. https://doi.org/10.1039/C3CC41605D

11. -Zhang L, Liu Y, Li X, Guo Y, Jiang Z, Jiao T, Yang J (2021) Synthesis of a new amino-furopyridine-based compound as a Novel fluorescent pH Sensor in Aqueous Solution. ACS Omega 6(7):4800–4806. https://doi.org/10.1021/acsomega.0c05734

12. -Xie H, Shao J, Yan Z, Ding J (2019) Furo[3,2-c]pyridine-Based Iridium Complex containing two methoxy groups for efficient solution-processed phosphorescent OLEDs. Asian J Org Chem 8(1):185–190. https://doi.org/10.1002/ajoc.201800657

13. -(a) Ghanem R, Yousef F, Abu Awwad O Effect of pH and β-cyclodextrin on the photophysical properties of lamotrigine. Turk J Chem 42(2): 247–256., Ghanem R, Baker H, Seif MA,

Al-Qawasmeh RA, Mataneh AA, Al-Gharabli SI (2010) Photochemical Transformation of Colchicine: A Kinetic Study. J Solution Chem 39(4): 441–456., Ghanem R (2015) Chemical Oxidation of Phthalmic Drug Timolol by Peroxodisulfate. Chem Sci Int J 8(3):1–14. https://doi.org/10.9734/ACSJ/2015/18782 (d), Ghanem R, Baker H, Al-Khazalah A, Matani A (2018) (2016) Spectroscopic and photophysical properties of terbutaline. JJC 11(3): 183–194

14. -Dennington R, Keith TA, Millam JM (2016) GaussView, Version 6. Semichem Inc., Shawnee Mission, KS, USA

15. -Frisch MJ, Trucks GW, Schlegel HB et al (2016) Gaussian 16, Revision C.01; Gaussian. Inc., Wallingford CT, USA

16. -Becke AD (1993) A new mixing of Hartree-Fock and density-functional theories. J Chem Phys 98:1372–1377. https://doi.org/10.1063/1.464304

17. -Ibrahim MM, Al-Refai M, Al-Fawwaz A, Ali BF, Geyer A, Harms K, Marsch M, Krüger M, Osman H, Azmi MN (2018) Synthesis of fluorescent 1-(3-Amino-4-(4-(tert-butyl)phenyl) – 6-(p-tolyl)furo[2,3-b]pyridin-2-yl)ethan-1-one: Crystal structure, fluorescence behavior, antimicrobial and antioxidant studies. J Fluoresc 28:655–662. https://doi.org/10.1007/s10895-018-2227-2

18. -Lechel T, Dash J, Brüdgam I, Reißig HU (2008) Novel furopyridine derivatives via Sonogashira reactions of Functionalized Pyridines. Eur J Org Chem 3647–3655. https://doi.org/10.1002/ejoc.200800398

19. -Grabowski ZR, Rubaszewska W (1977) Generalised Förster cycle. Thermodynamic and Extrathermodynamic Relationships between Proton transfer, Electron transfer and electronic excitation. J Chem Soc Faraday Trans 1:73: 11–28. https://doi.org/10.1039/F19777300011

20. -Wierzchowski J (2014) Excited-state Proton transfer and phototautomerism in nucleobase and nucleoside analogs: a Mini-Review. Nucleosides Nucleotides Nucleic Acids 33(9):626–644. https://doi.org/10.1080/15257770.2014.913065

21. -Valeur B (2001) Molecular fluorescence: principles and applications. Wiley-VCH, Germany

22. -Lippert VE (1955) Dipolmoment und Elektronenstruktur von angeregten Molekülen. Z Naturforschg 10a:541–545. https://doi.org/10.1515/zna-1955-0707

23. -Mataga N, Kaifu Y, Kolzumi M (1956) Solvent Effects upon fluorescence Spectra and the dipolemoments of excited molecules. Bull Chem Soc Jpn 29(4):465–470. https://doi.org/10.1246/bcsj.29.465

24. -Melavanki RM, Patil HD, Umapathy S, Kadadevarmath JS (2012) Solvatochromic Effect on the Photophysical Properties of two coumarins. J Fluoresc 22:137–144. https://doi.org/10.1007/s10895-011-0939-7

25. -Nishiyama K, Watanabe Y, Yoshida N, Hirata F (2012) Solvent Effects on Electronic Structures of Coumarin 153: parallel studies by means of Spectroscopy and RISM-SCF calculations. J Phys Soc Jpn 81:SA016. https://doi.org/10.1143/JPSJS.81SA.SA016

26. -Mannekutla JR, Mulimani BG, Inamdar SR (2008) Solvent effect on absorption and fluorescence spectra of coumarin laser dyes: evaluation of ground and excited state dipole moments. Spectrochim Acta A Mol Biomol Spectrosc 69(2):419–426. https://doi.org/10.1016/j.saa.2007.04.016

27. -Marcus Y (1998) The Properties of Solvents - Wiley Series in Solution Chemistry: volume 4. John Wiley & Sons Ltd, England

28. -Kamlet MJ, Dickinson C, Taft RW (1981) Linear Solvation Energy Relationships. Solvent Effects on some fluorescence probes. Chem Phys Lett 77(1):69–72. https://doi.org/10.1016/0009-2614(81)85602-3

29. -Kamlet MJ, Abboud JLM, Abraham MH, Taft RW (1983) Linear Solvation Energy Relationships. 23. A Comprehensive Collection of the Solvatochromic Parameters, $\pi^*$, $\alpha$, and $\beta$, and some methods for simplifying the generalized Solvatochromic equation. J Org Chem 48(17):2877–2887. https://doi.org/10.1021/jo00165a018

30. -Chipem FAS, Mishra A, Krishnamoorthy G (2012) The role of hydrogen bonding in excited state intramolecular charge transfer. Phys Chem Chem Phys 14:8775–8790. https://doi.org/10.1039/C2CP23879A

31. -Chai S, Zhao GJ, Song P, Yang SQ, Liu JY, Han KL (2009) Reconsideration of the excited-state double proton transfer (ESDPT) in 2-aminopyridine/acid systems: role of the intermolecular hydrogen bonding in excited states. Phys Chem Chem Phys 11:4385–4390. https://doi.org/10.1039/B816589K

32. -Carmona C, Galán M, Angulo G, Muñoz MA, Guardado P, Balón M (2000) Ground and singlet excited state hydrogen bonding interactions of betacarbolines. Phys Chem Chem Phys 2:5076–5083. https://doi.org/10.1039/B005455K

33. -Ihmels H, Schäfer K (2009) Excited-state acidity of the 8-hydroxyacridizinium ion—a water-soluble photoacid. Photochem Photobiol Sci 8:309–311. https://doi.org/10.1039/B816048A

34. -Yousef F, Ghanem R, Al-Sou'od K, Alsarhan A, Abuflaha R, Bodoor K, Assaf K, El-Barghouthi M (2021) Investigation of spectroscopic properties and molecular dynamics simulations of the interaction of mebendazole with β-cyclodextrin. J Iraan Chem Soc 18:75–86. https://doi.org/10.1007/s13738-020-02006-w